Numerical modelling of transient-electromagnetic fields in three-dimensional conductors: A comparative study

Peter Weidelt
Institute of Geophysics and Meteorology
Technical University of Braunschweig, Germany

Introduction

The computation of transient electromagnetic fields in three-dimensional conductors is an important technique for the interpretation of transient electromagnetic data in applied geophysics. In the present study we will review the current methods of computation.

For computing transient 3-D fields we have the choice between at least three modelling techniques:

- **Modelling in the frequency domain followed by a Fourier transform into the time domain**
  For a suitable number n_f (approx. 20 - 30) of logarithmically equidistant frequencies we compute the 3-D frequency response and transform it by a Fast Hankel Transform into the time domain. Although excellent 3-D frequency domain codes are freely available (e.g. from Randy Mackie), the requirement of n_f 3-D forward models drastically speeds down its performance. This method will not be considered in this study.

- **Continuation of initial values by time-stepping (FDTD)**
  Assuming a shut-off of sources $t = 0$, we continue the initial values at time $t = 0^+$ to time $t > 0$. Whereas explicit FDTD time stepping methods for the diffusion equation are stable only for very small time steps, explicit FDTD methods with a reasonable time step become possible introducing a fictitious displacement current. The Courant-Friedrichs criterion still imposes an upper limit on time step Δt, which, however, can increase with time. The presentation in this study is mostly based on Wang & Hohmann (1993).

- **Continuation of the initial field with spectral finite differences (SLDM)**
  This method (Spectral Lanczos Decomposition Method) has been developped by Druskin & Knizhnerman (1988). The initial values are approximated by a system of orthogonal decay modes ('Ritz vectors') with decay constants ('Ritz values'), resulting as eigenvectors and eigenvalues from a low dimensional subspace approximation of the high dimensional system matrix. The evolution of the fields for $t > 0$ is then easily available. The dimension of the subspace required for convergence significantly increases with time.

1. Model Description

1.1 Basic Equations and Spatial Discretization

The basic equations read in the quasistatic approximation

$$\nabla \times \mathbf{E} = -\dot{\mathbf{B}}, \tag{1}$$

$$\nabla \times \mathbf{B} = \mu_0(\sigma\mathbf{E} + \mathbf{J}^e), \tag{2}$$

or after elimination of $\mathbf{B}$

$$\nabla \times \nabla \times \mathbf{E} + \mu_0\sigma\dot{\mathbf{E}} = -\mu_0\dot{\mathbf{J}}^e. \tag{3}$$

$\mathbf{E}$ and $\mathbf{B}$ are the vectors of the electric and magnetic field and $\mathbf{J}^e$ is the source current density, which is shut-off at time $t = 0$. The dotted variables denote time derivatives.

We assume Cartesian coordinates with z pointing downwards. The Earth with the locally varying conductivity $\sigma(\mathbf{r}) > 0$ occupies the half-space $z > 0$. The air half-space $z < 0$ is assumed to be non-conducting. For the spatial discretization we use Yee cells (Yee 1966), in which the electric field components are localized at the edges of the prismatic cell and the magnetic field components in the centers of the faces of the cell (see. Fig. 1).

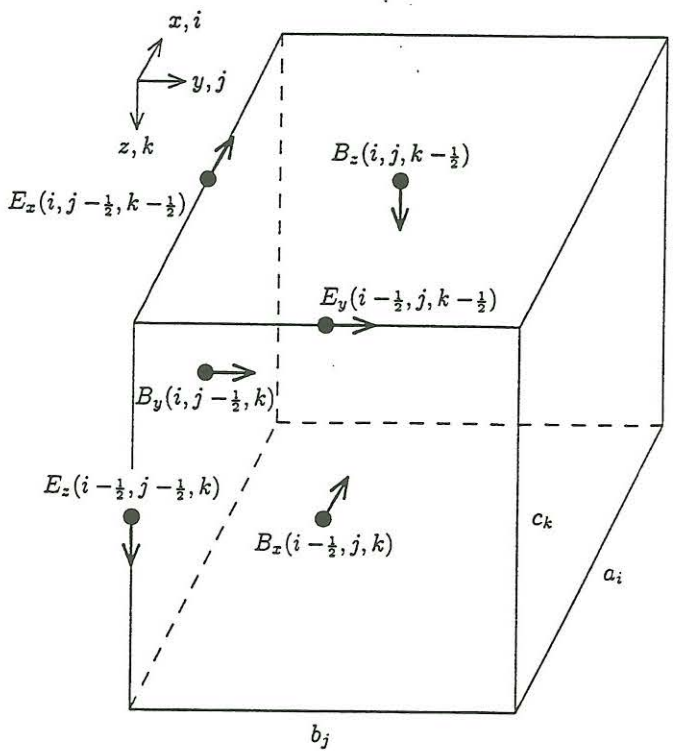

Fig. 1: Localization of the electromagnetic field components in the Yee cell

1.2 Spatial Averages of Conductivities

When casting the basic equations into their finite difference version, we integrate, e.g., the x-component of (2) over a prism with dimension a_i in x-direction, $b_{j+\frac{1}{2}}$ in y-direction and $c_{k+\frac{1}{2}}$ in z-direction (see Fig. 2). The prism is centered around $E_x(i, j+\frac{1}{2}, k+\frac{1}{2})$ and calculate the arithmetic average of the conductivity $\overline{\sigma}_x(i, j+\frac{1}{2}k+\frac{1}{2})$ along the current path (Fig. 2)

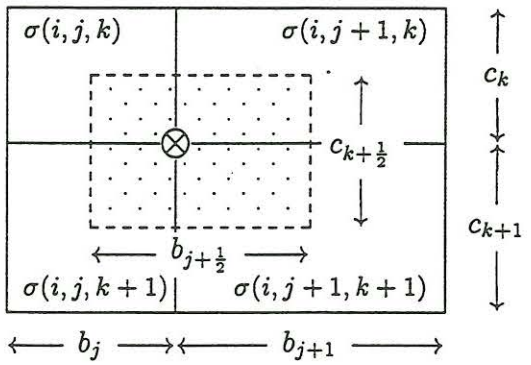

Fig. 2: Geometry for averaging conductivities with current flow in x-direction. The averaging area is shaded.

1.3 Boundary Conditions

The conductivity distribution in the Earth $z > 0$ is assumed to be confined to the prism Ω

$$\Omega = \begin{cases} 0 \le x \le L_x, \\ 0 \le y \le L_y, \\ 0 \le z \le L_z \end{cases}$$

with perfectly conducting walls except at $z = 0$. Therefore we put at the boundaries $\partial\Omega$ inside the Earth

$$\hat{\mathbf{n}} \times \mathbf{E} = \mathbf{0}, \qquad \mathbf{r} \in \partial\Omega.$$

This boundary condition implies on using (1)

$$\hat{\mathbf{n}} \cdot \mathbf{B} = 0, \qquad \mathbf{r} \in \partial\Omega.$$

At the boundary $z = 0$ to the air-halfspace we apply an integral boundary condition in $\mathbf{B}$, which saves the treatment of the air-halfspace $z < 0$. This boundary condition expresses $\hat{\mathbf{z}} \times \mathbf{B}$ in the level $z = -c_1/2$ through $\hat{\mathbf{z}} \cdot \mathbf{B} = B_z$ in the level $z = 0$. Since $\nabla \times \mathbf{B} = 0$ in $z < 0$, $\mathbf{B}$ is a potential field, $\mathbf{B} = -\nabla\Phi$, which implies

$$\Phi(\mathbf{r}_0) = \frac{1}{2\pi} \int\int_{-\infty}^{+\infty} \frac{\hat{\mathbf{z}} \cdot \nabla\Phi(\mathbf{r})\, d^2\mathbf{r}}{|\mathbf{r} - \mathbf{r}_0|}$$

yielding

$$B_x(\mathbf{r}_0) = \frac{1}{2\pi} \int\int_{-\infty}^{+\infty} \frac{(x - x_0) B_z(\mathbf{r})}{|\mathbf{r} - \mathbf{r}_0|^3}\, d^2\mathbf{r}, \tag{4}$$

$$B_y(\mathbf{r}_0) = \frac{1}{2\pi} \int\int_{-\infty}^{+\infty} \frac{(y - y_0) B_z(\mathbf{r})}{|\mathbf{r} - \mathbf{r}_0|^3}\, d^2\mathbf{r} \tag{5}$$

with $\mathbf{r} := (x, y, 0)$ and $\mathbf{r}_0 := (x_0, y_0, -c_1/2)$. These are the boundary conditions applied for FDTD (see Sect. 2.2). For SLDM (Sect. 3.2) we use a boundary condition in $\mathbf{E}$, which is obtained from (4) and (5) by (1), i.e. by $\nabla \times \mathbf{E} = -\dot{\mathbf{B}}$:

$$\partial_y E_z(\mathbf{r}_0) - \partial_z E_y(\mathbf{r}_0) = \frac{1}{2\pi} \int\int_{-\infty}^{\infty} \{\partial_x E_y(\mathbf{r}) - \partial_y E_x(\mathbf{r})\} \frac{(x - x_0)\, d^2\mathbf{r}}{|\mathbf{r} - \mathbf{r}_0|^3}, \tag{6}$$

$$\partial_z E_x(\mathbf{r}_0) - \partial_x E_z(\mathbf{r}_0) = \frac{1}{2\pi} \int\int_{-\infty}^{\infty} \{\partial_x E_y(\mathbf{r}) - \partial_y E_x(\mathbf{r})\} \frac{(y - y_0)\, d^2\mathbf{r}}{|\mathbf{r} - \mathbf{r}_0|^3}. \tag{7}$$

In practice, the infinite range of integration is restricted to a finite range and the resulting discretized convolution integrals are easily evaluated by an FFT.

1.4 Initial Conditions

The source is assumed to lie in $z \ge 0$ and is shut-off at $t = 0$, i.e.

$$\mathbf{J}^e(t) = \mathbf{J}^e(t = 0^-) \cdot \Theta(-t), \quad \dot{\mathbf{J}}^e(t) = -\mathbf{J}^e(t = 0^-) \cdot \delta(t)$$

where $\Theta(t)$ is the Heaviside function and $\delta(t)$ the Dirac delta function. Integrating the basic equation (3) between $t = 0^-$ and $t = 0^+$, we obtain

$$\mathbf{E}(t = 0^+) = \mathbf{E}(t = 0^-) + (1/\sigma)\mathbf{J}^e(t = 0^-) + [1/(\mu_0\sigma)] \cdot [\nabla \times \mathbf{B}(t = 0^+) - \nabla \times \mathbf{B}(t = 0^-)].$$

For an inductive source the electric field is initially mostly confined to the position of the loop, where - by Lenz's rule - the induced current try to counteract the current shut-off and therefore flow in the same direction as the source currents at $t = 0^-$. The second RHS term takes into account the induced currents outside the source immediately after the shut-off. In a uniform *full space* the induced fields show the typical $\exp[-\mu_0\sigma R^2/(4t)]$ behaviour (with R as separation between source and measuring point) and therefore would vanish for $t \to 0^+$). However, due to the presence of the insolating air-halfspace ($\sigma = 0$) one observes for all points at the surface $z = 0$ a signal also for $t = 0^+$. This signal rapidly decays with depth $\sim \exp([-\mu_0\sigma z^2/(4t)]$ and therefore will be small when integrated over a vertical grid width. To a first approximation it is neglected.

Therefore the initial conditions are

a) for an **inductive** source (loop) with $\mathbf{E}(t = 0^-) = 0$

$$\boxed{\mathbf{E}(t = 0^+) = (1/\sigma)\mathbf{J}^e(t = 0^-)} \tag{8}$$

b) for a **galvanic-inductive** source (grounded electric dipole) with $\mathbf{E}(t = 0^-) = -\nabla\Phi$ as direct current field

$$\boxed{\mathbf{E}(t = 0^+) = -\nabla\Phi + (1/\sigma)\mathbf{J}^e(t = 0^-)} \tag{9}$$

2. FDTD Time-Stepping

2.1 Artificial Displacement Current and Constraints on the Time Step

A continuation of the initial electric field $\mathbf{E}(t = 0^+)$ by means of the diffusion type basic equation (3)

$$\nabla \times \nabla \times \mathbf{E} + \mu_0\sigma\dot{\mathbf{E}} = \mathbf{0}$$

after the simple Euler method

$$\mathbf{E}(t + \Delta t) = \mathbf{E}(t) - \nabla \times \nabla \times \mathbf{E}(t) \cdot \frac{\Delta t}{\mu_0\sigma}$$

is stable only, if the time step Δt is sufficiently small. If Δs is the spatial discretization of the $\nabla \times \nabla\times$-operator, then in the simplest case of a uniform full space the condition

$$\Delta t \leq \mu_0\sigma\Delta s^2/4$$

has to be satisfied (e.g. Oristaglio & Hohmann, 1984). For $\sigma = 0.01$ S/m and $\Delta s = 10$ m we obtain $\Delta t = 3 \cdot 10^{-7}$ s.

Following Du Fort & Frankel (1953), Oristaglio & Hohmann (1984) and Wang & Hohmann (1993) a greater time step is possible by introducing a **fictitious displacement current** $\gamma\dot{\mathbf{E}}$. Then Eq. (3) is modified to

$$\nabla \times \nabla \times \mathbf{E} + \mu_0(\sigma\dot{\mathbf{E}} + \gamma\ddot{\mathbf{E}}) = \mathbf{0} \tag{10}$$

Instead of solving this second order equation in time and space, Wang & Hohmann (1993) propose to solve the coupled first order system

$$\gamma\dot{\mathbf{E}} = -\sigma\mathbf{E} + \nabla \times \mathbf{B}/\mu_0 \tag{11}$$

$$\dot{\mathbf{B}} = -\nabla \times \mathbf{E}. \tag{12}$$

Let Δt be the time step and $t_n := n \cdot \Delta t$. Then $\mathbf{E}$ is determined for integer n and $\mathbf{B}$ for half-integer n,

$$\boxed{\mathbf{E}^n \Rightarrow_{Eq.(12)} \mathbf{B}^{n+\frac{1}{2}} \Rightarrow_{Eq.(11)} \mathbf{E}^{n+1}} \tag{13}$$

If Δs_{min} is the smallest grid spacing, then the Du Fort-Frankel method is stable if

$$\boxed{\gamma \geq \frac{3}{\mu_0}\left(\frac{\Delta t}{\Delta s_{min}}\right)^2 \quad \text{or} \quad v := \frac{1}{\sqrt{\mu_0\gamma}} \leq \frac{\Delta s_{min}}{\sqrt{3}\Delta t}} \tag{14}$$

This corresponds to the Courant-Friedrichs criterion, which states that the grid velocity $\Delta s/\Delta t$ should be greater than $\sqrt{D}$ times the wave velocity v, where D is the dimensionality of the problem (here $D = 3$). Without fictitious displacement current ($\gamma = 0$), the wave velocity is infinite and the Courant-Friedrichs criterion cannot be satisfied.

In classical electrodynamics the diffusive character of the field prevails after an impulsive excitation at $t = 0$ for time lags much greater than $2\epsilon/\sigma$, which is twice the free decay time of charges. Replacing ϵ by γ this means on using (14) that the diffusive field character is conserved for

$$t \gg 2\gamma/\sigma_{min} \geq \frac{6}{\mu_0 \sigma_{min}} \cdot \left(\frac{\Delta t}{\Delta s_{min}}\right)^2$$

or

$$\boxed{\Delta t \ll \sqrt{\mu_0 \sigma_{min} t/6}\, \Delta s_{min}} \tag{15}$$

[Oristaglio & Hohmann (1984), Ahidjaja & Hohmann (1989), Wang & Hohmann (1993)]. Putting

$$\Delta t = \alpha \sqrt{\mu_0 \sigma_{min} t}\, \Delta s_{min},$$

the numerical experiments of Wang & Hohmann have shown that $\alpha = 0.05...0.1$ gives already very satisfactory results. The time steps can increase with time. From

$$\frac{\Delta t}{\Delta n} = \beta \sqrt{t}, \quad \beta := \alpha \sqrt{\mu_0 \sigma_{min}}\, \Delta s_{min}$$

we obtain by integration the approximate number $n(t)$ of time steps required to reach the time t, starting at t_0,

$$\boxed{n(t) \simeq \frac{2}{\beta} \cdot (\sqrt{t} - \sqrt{t_0})} \tag{16}$$

2.2 The Time-Stepping Equations

In this section we shall derive the the time-stepping equations for the coupled system (11) and (12). According to (13) the electric field is computed at integer time steps $n\Delta t$ and the magnetic field at half-integer time steps $(n + \frac{1}{2})\Delta t$.

We start with the update of the magnetic field. The x-component of (12) reads

$$\dot{B}_x = \frac{\partial E_y}{\partial z} - \frac{\partial E_z}{\partial y}$$

or discretized in time

$$B_x^{n+\frac{1}{2}} = B_x^{n-\frac{1}{2}} + \left(\frac{\partial E_y}{\partial z} - \frac{\partial E_z}{\partial y}\right)^n \Delta t. \tag{17}$$

For non-uniform time spacing Δt is replaced by $(\Delta t_{n-1} + \Delta t_n)/2$. Considering the spatial discretization, Eq. (17) is extended to

$$\begin{aligned} &B_x^{n+\frac{1}{2}}(i+\tfrac{1}{2}, j, k) = B_x^{n-\frac{1}{2}}(i+\tfrac{1}{2}, j, k) \\ &+ \left(\frac{E_y(i+\frac{1}{2}, j, k+\frac{1}{2}) - E_y(i+\frac{1}{2}, j, k-\frac{1}{2})}{c_k} - \frac{E_z(i+\frac{1}{2}, j+\frac{1}{2}, k) - E_z(i+\frac{1}{2}, j-\frac{1}{2}, k)}{b_j}\right)^n \Delta t. \end{aligned}$$

Wang & Hohmann (1993) point out that the magnetic solenoidal condition $\nabla \cdot \mathbf{B} = 0$, which in theory should be inforced by Faraday's law (1) by imposing the intial condition $\nabla \cdot \mathbf{B}(t = 0) = 0$, is in fact easily violated at late time because $\mathbf{E}$ approaches a potential field, such that $\nabla \times \mathbf{E} \simeq \mathbf{0}$. Therefore they propose to satisfy the solenoidal condition explicitly by replacing B_z-update by

$$\begin{aligned} &B_z^{n+\frac{1}{2}}(i, j, k+\tfrac{1}{2}) = B_z^{n+\frac{1}{2}}(i, j, k-\tfrac{1}{2}) \\ &-c_k \left(\frac{B_x(i+\frac{1}{2}, j, k) - B_x(i-\frac{1}{2}, j, k)}{a_i} - \frac{B_y(i, j+\frac{1}{2}, k) - B_y(i, j-\frac{1}{2}, k)}{b_j}\right)^{n+\frac{1}{2}}. \end{aligned}$$

In our implementation we are taking a weighted mean of both versions, posing at later time higher weights onto the latter.

Turning now to the time-stepping of the electric field, we consider the x-component of (11)

$$\gamma \dot{E}_x + \sigma E_x = \frac{1}{\mu_0}\left(\frac{\partial B_z}{\partial y} - \frac{\partial B_y}{\partial z}\right).$$

and integrate it over t from t_n to t_{n+1},

$$\gamma\left(E_x^{n+1} - E_x^n\right) + \frac{\sigma\Delta t}{2}\left(E_x^n + E_x^{n+1}\right) = \frac{\Delta t}{\mu_0}\left(\frac{\partial B_z}{\partial y} - \frac{\partial B_y}{\partial z}\right)^{n+\frac{1}{2}}. \tag{18}$$

This yields the electric field time-stepping formula

$$E_x^{n+1} = k_1 E_x^n + k_2\left(\frac{\partial B_z}{\partial y} - \frac{\partial B_y}{\partial z}\right)^{n+\frac{1}{2}} \tag{19}$$

with

$$k_1 = \frac{2\gamma - \sigma\Delta t}{2\gamma + \sigma\Delta t}, \quad k_2 = \frac{2\Delta t/\mu_0}{2\gamma + \sigma\Delta t}.$$

The spatial derivatives are approximated using the staggered grid geometry of Fig. 1 and averaged conductivities are introduced.

When applying the time stepping equations derived above, it is used that the tangential electric field and the normal magnetic field is vanishing at the perfectly conducting boundaries inside the Earth (see Sect. 1.2). A problem arises when time stepping the tangential electric field at the surface of the Earth. Here E_x requires B_y half a grid width **above** the air-earth interface and E_y requires B_x at the same level inside the air-halfspace. These values are obtained using using the integral boundary conditions (4) and (5) and evaluating them by an FFT.

2.3 The Initial Condition

In Sect. 1.3 we have advocated as initial condition the electric and magnetic field, which essentially are copies of the field at $t = 0^-$ prior to shut-off. Because of the introduction of the artificial displacement currents this might no longer be a good choice. Therefore we are following Hohmann & Wang (1993) and and calculate the diffusive field at a short time t_0 after shut-off, when the 'smoke rings of the source' are about one grid width below the surface. Hence our choice is

$$t_0 = \mu_0\sigma_0 c_1^2,$$

where σ_0 is the background conductivity and c_1 is the grid spacing in the uppermost part of the grid. By selecting σ_0, it is assumed that there are no outcropping conductivity anomalies. Otherwise t_0 has to be adjusted to this situation! More specific, the electric field should be calculated for t_0 and the magnetic field for $t_0 + \Delta t/2$. - For $\sigma_0 = 0.01$ S/m and $c_1 = 10$ m we have $t_0 \simeq 10^{-6}$ s.

2.4 Numerical Example

We finnish the presentation of the time stepping method with a numerical example (Fig. 3). The conductor is a 1D model consisting of a 330 m thick 10 Ωm-layer at a depth of 30 m immersed in a uniform halfspace of 100 Ωm. The transmitter stands over the center of the conductor. The crosses show the results of FDTD for three time lags along a central profile. These results are compared with the analytical 1D model (full lines). The agreement is acceptable. The model consisted of 64 cells in all three directions (oversampled in the vertical direction) and has required 1000 time steps.

Fig. 3: Comparison of numerical 3D-results with analytical 1D-data. Shown are the central profiles over the loop for three time lags. The agreement is satifactory, but could be better.

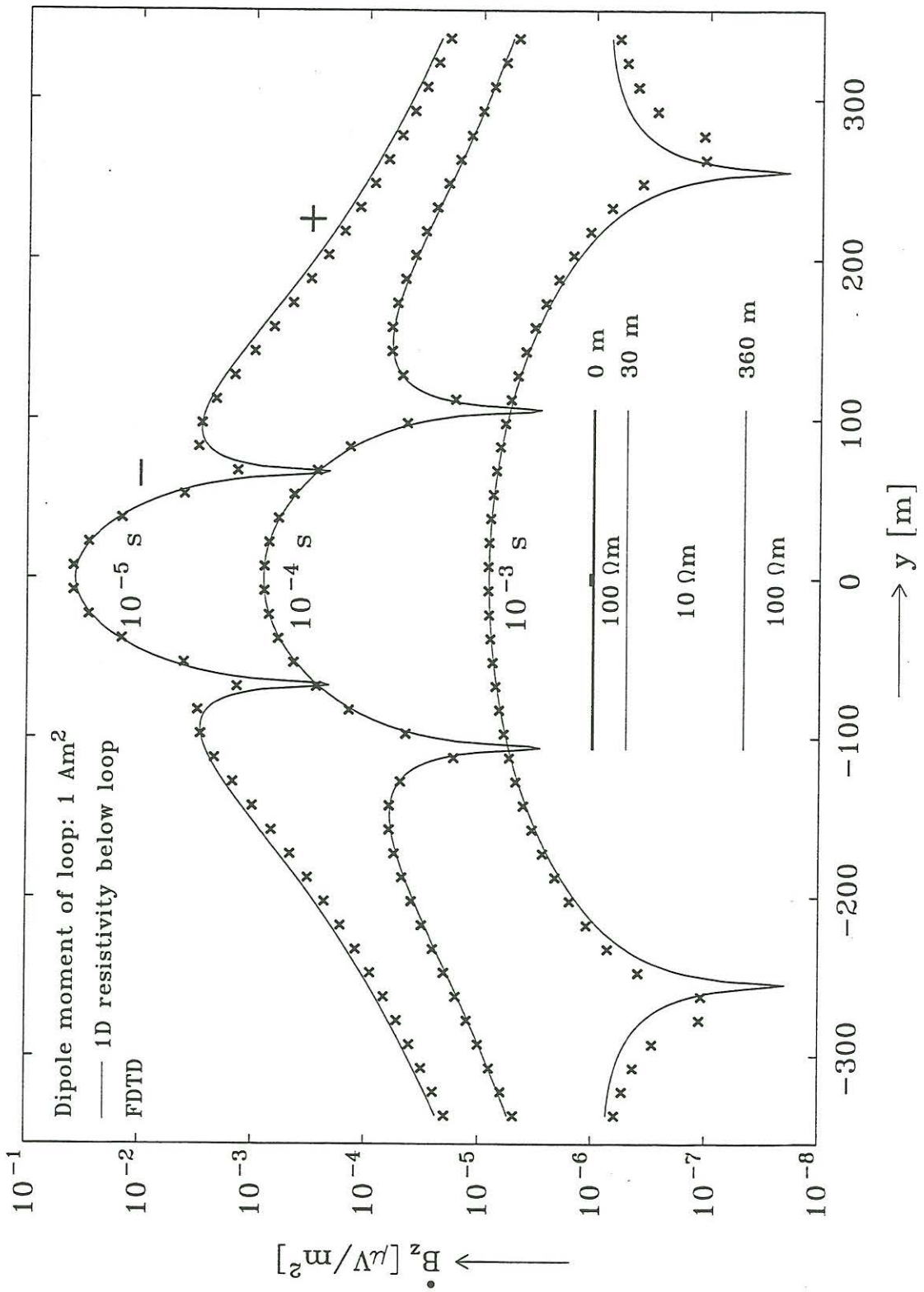

3. The Spectral Finite Difference Method

3.1 Introductory Remarks

This method has been developped by Druskin & Knizhnerman (1988). The initial values are approximated by a system of orthogonal decay modes ('Ritz vectors') with decay constants ('Ritz values'), resulting as eigenvectors and eigenvalues from a low dimensional subspace approximation of the high dimensional system matrix. The evolution of the fields for $t > 0$ is then easily available. The key procedure is the subspace approximation of the system matrix by the Lanczos method. A construction of an orthonormal set of approximation vectors is only possible with 'infinite precision arithmetics'. In practice the orthonormality is destroyed after a few (10 - 20) iterations ('Lanczos phenomenon'), see e.q. Parlett (1980), Grubert (1992). Fortunately the Lanczos phenomenon does not make the Lanczos process inapplicable, it only increases the required dimension of the subspace to reach convergence at late time. Papers related to the spectral finite difference method are Druskin & Knizhnerman (1994), Druskin *et al.* (1999), Hördt *et al.* (1992), Árnason (1999) and Remis & van den Berg (1997,1998). The paper of Druskin *et al.* (1999) is of particular interest, because it shows a way to circumvent the poor convergence properties at late time by basing the subspace iteration on the inverse of the system matrix.

3.2 The System Matrix

The system matrix is the FD-version of the basic equation (3). This equation connects thirteen field components, such that the system matrix has at most thirteen entries in each row or column. Due to the self-adjoint $\nabla \times \nabla \times$-operator (including boundary conditions) the system matrix is symmetric.

The symmetry is conserved by the transformations

$$e_x(i,j+\tfrac{1}{2},k+\tfrac{1}{2}) := \sqrt{\mu_0 a_i b_{j+\frac{1}{2}} c_{k+\frac{1}{2}} \overline{\sigma}_x(i,j+\tfrac{1}{2},k+\tfrac{1}{2})}\, E_x(i,j+\tfrac{1}{2},k+\tfrac{1}{2}), \tag{20}$$

$$e_y(i+\tfrac{1}{2},j,k+\tfrac{1}{2}) := \sqrt{\mu_0 b_j c_{k+\frac{1}{2}} a_{i+\frac{1}{2}} \overline{\sigma}_y(i+\tfrac{1}{2},j,k+\tfrac{1}{2})}\, E_y(i+\tfrac{1}{2},j,k+\tfrac{1}{2}), \tag{21}$$

$$e_z(i+\tfrac{1}{2},j+\tfrac{1}{2},k) := \sqrt{\mu_0 c_k a_{i+\frac{1}{2}} b_{j+\frac{1}{2}} \overline{\sigma}_z(i+\tfrac{1}{2},j+\tfrac{1}{2},k)}\, E_z(i+\tfrac{1}{2},j+\tfrac{1}{2},k). \tag{22}$$

The weights are essentially the square root of the conductivity integrated over the prism centered around the electric field component in the staggered grid approximation of Fig. 1.

For a basic domain consisting of cell numbers n_x, n_y and n_z in x-, y- and z-direction the number N of nontrivial field components (i.e. excluding the vanishing tangential field components at the perfectly conducting walls) is easily counted:

$$N = n_x(n_y-1)n_z + (n_x-1)n_y n_z + (n_x-1)(n_y-1)n_z.$$

Assembling the N nontrivial electric field components in the N-dimensional vector $\underline{f}$ and denoting the transformed $N \times N$ system matrix by $\underline{\underline{A}}$, the basic equation (3) reduces for $t > 0$ to a system of evolution equations for $\underline{f}(t)$ with the initial condition $\underline{f}(0^+) =: \underline{f}_0$,

$$\boxed{\underline{\underline{A}}\,\underline{f}(t) + \dot{\underline{f}}(t) = 0, \quad t > 0, \qquad \underline{f}(0^+) = \underline{f}_0} \tag{23}$$

The matrix $\underline{\underline{A}}$ has the following properties

- symmetric
- non-negative eigenvalues
- high dimensional ($N \simeq 3n_x n_y n_z \simeq 10^5$ to 10^6)
- sparse (at most 13 entries per row or column (apart from E_x and E_y at the air-earth interface, see below)

If $\underline{\phi}_n$ and λ_n are the eigenvectors and eigenvalues of $\underline{\underline{A}}$, then the exact solution of (23) is

$$\underline{f}(t) = \sum_{n=1}^{N} (\underline{\phi}_n^T \underline{f}_0)\underline{\phi}_n \exp(-\lambda_n t). \tag{24}$$

In practice, however, the eigenvectors and eigenvalues of this high dimensional matrix are difficult to obtain. Therefore a recourse to approximate solutions is required. Before doing this we look at the treatment of the air halfspace.

The first equation of Sect. 3.2 shows that $\dot{E}_x$ at $z = 0$ is connected with $\dot{B}_y$ at half the vertical width in the air-halfspace, i.e. at $z = -c_1/2$. Our task ist to express

$$\dot{B}_y = \frac{\partial E_z}{\partial x} - \frac{\partial E_x}{\partial z}$$

at $z = -c_1/2$ in terms of E_x and E_y at $z = 0$, which is formally solved by (7). This formula is equivalent to (5). In this case E_x and E_y at the surface are connected with all $n_x(n_y - 1) + (n_x - 1)n_y$ surface values of E_x and E_y.

3.3 The Lanczos Method

In practice, an approximate solution of (23) is sought in an M-dimensional subspace of the N-dimensional space spanned by $\underline{\underline{A}}$. This subspace is defined by the Krylov vectors

$$\underline{f}_0, \quad \underline{\underline{A}}\,\underline{f}_0, \quad \underline{\underline{A}}^2\underline{f}_0, \quad \underline{\underline{A}}^3\underline{f}_0, \ \cdots, \ \underline{\underline{A}}^{M-1}\underline{f}_0$$

as suggested by

$$\underline{f}(t) = \exp(-t\underline{\underline{A}})\underline{f}_0 = \sum_{m=0}^{\infty} \frac{1}{m!}(-t\underline{\underline{A}})^m \underline{f}_0.$$

Although this series is convergent for all $t > 0$, it is applicable only for moderate values of $t\lambda_{max}$, since otherwise the (small) result drowns in numerical errors due to fact that the terms in the series (with alternating signs!) first increase to very high values until $1/m!$ pulls them down. The intricacy of computing matrix exponentials is discussed by Moler & van Loan (1978).

From the M Krylov vectors is formed an orthonormal Basis

$$\underline{q}_1, \cdots, \underline{q}_M,$$

which is formally achieved by the elegant Lanczos process [e.g. Parlett (1980), Grubert (1992)]. It is based on the observation that

$$\boxed{\underline{\underline{A}}\,\underline{q}_i = \underline{q}_{i-1}\beta_{i-1} + \underline{q}_i\alpha_i + \underline{q}_{i+1}\beta_i} \tag{25}$$

leading to the following algorithm:

Let $\underline{r}_0 := \underline{f}_0$ and $\beta_0 = |\underline{f}_0| \neq 0$. Then we have for $j = 1, 2, .., M$

$$\begin{aligned}
\underline{q}_j &= \underline{r}_{j-1}/\beta_{j-1} \\
\underline{u}_j &= \underline{\underline{A}}\,\underline{q}_j \\
\underline{r}_j &= \underline{u}_j - \underline{q}_{j-1}\beta_{j-1} \qquad (\underline{q}_0 = 0) \\
\alpha_j &= \underline{q}_j^T\,\underline{r}_j \\
\underline{r}_j &= \underline{r}_j - \alpha_j\underline{q}_j \\
\beta_j &= |\underline{r}_j|
\end{aligned}$$

With $\underline{\underline{Q}} := (\underline{q}_1, \cdots, \underline{q}_M)$, $\underline{\underline{Q}}^T\underline{\underline{Q}} = \underline{\underline{I}}_M$, where $\underline{\underline{I}}_M$ is the M-dimensional unit matrix, we have as a consequence of (25)

$$\underline{\underline{A}}\,\underline{\underline{Q}} = \underline{\underline{Q}}\,\underline{\underline{H}} + \underline{\underline{R}},$$

where $\underline{\underline{H}}$ is the tridiagonal matrix

$$\underline{\underline{H}} = \begin{pmatrix}
\alpha_1 & \beta_1 & & & & \\
\beta_1 & \alpha_2 & \beta_2 & & & \\
 & \ddots & \ddots & \ddots & & \\
 & & \ddots & \ddots & \ddots & \\
 & & & \beta_{M-2} & \alpha_{M-1} & \beta_{M-1} \\
 & & & & \beta_{M-1} & \alpha_M
\end{pmatrix}$$

and $\underline{\underline{R}}$ the remainder

$$\underline{\underline{R}} = \beta_M \underline{q}_{M+1}(0, 0, ..., 1),$$

where the last vector has M elements. With the approximation

$$\underline{\underline{A}}\,\underline{\underline{Q}} \simeq \underline{\underline{Q}}\,\underline{\underline{H}} \tag{26}$$

and the ansatz

$$\underline{f}(t) = \underline{\underline{Q}}\,\underline{\chi}(t) = \sum_{j=1}^{M} \underline{q}_j \chi_j(t)$$

(23) is reduced to the much simpler M-dimensional tridiagonal problem

$$\boxed{\underline{\underline{H}}\,\underline{\chi}(t) + \dot{\underline{\chi}}(t) = 0, \quad \underline{\chi}(0^+) = |\underline{f}_0|(1, 0, 0, ..., 0)^T}$$

taking into account that $\underline{f}_0 = |\underline{f}_0|\underline{q}_1$. In analogy to (24) this problem is solved by

$$\underline{\chi}(t) = \sum_{m=1}^{M} \gamma_m \underline{s}_m \exp(-\vartheta_m t), \quad \gamma_m := |\underline{f}_0| s_{1m},$$

where $\underline{s}_m$ and ϑ_m are the eigenvectors and eigenvalues of $\underline{\underline{H}}$. Summarizing we have

$$\boxed{\underline{f}(t) \simeq \sum_{j=1}^{M} \underline{q}_j \chi_j(t) = \sum_{m=1}^{M} \gamma_m \underline{\psi}_m \exp(-\vartheta_m t)}$$

with

$$\chi_m(t) = \sum_{m=1}^{M} \gamma_m s_{jm} \exp(-\vartheta_m t), \quad \underline{\psi}_m = \underline{\underline{Q}}\,\underline{s}_m.$$

The *Ritz vectors* $\underline{\psi}_m$ with $\underline{\psi}_m^T \underline{\psi}_n = \delta_{mn}$ are approximate orthogonal decay modes with the *Ritz values* ϑ_m as decay constants.

The orthogonality of the Ritz vectors is in view of the symmetry transformations (20) to (22) an expression of the weighted orthogonality of decay modes $\mathbf{E}_m(\mathbf{r})$ and $\mathbf{E}_m(\mathbf{r})$ in the continuum description,

$$\int_\Omega \mathbf{E}_m(\mathbf{r}) \cdot \mathbf{E}_n(\mathbf{r})\, \sigma(\mathbf{r})\, d^3\mathbf{r} = \delta_{mn}.$$

Due to numerical approximations, the decay constants can become even slightly negative. In practice [see also Druskin & Knizhnerman (1994)] we ignore all eigenvalues (and corresponding eigenvectors) below a certain threshold, which is given by an estimate of the smallest decay constant,

$$\vartheta_{min} \geq \frac{\pi^2}{\mu_0 \sigma_{max} L_{max}^2},$$

where L_{max} is the greatest dimension (space diagonal!) of the model.

3.4 Convergence Estimates

The computational load of the spectral finite difference technique depends on the dimension N of the matrix $\underline{\underline{A}}$ and the dimension M of the approximating subspace and is mostly required to the M-fold computation of the product $\underline{\underline{A}}\,\underline{q}_j$ in the Lanczos process. For fixed N the efficiency of the spectral method therefore depends on the dimension M. Druskin & Knizhnerman (1988, 1994) show that in exact arithmetics

$$M \gg \sqrt{\vartheta_{max} t_{max}} > \frac{4}{\Delta s_{min}} \sqrt{\frac{t_{max}}{\mu_0 \sigma_{min}}}.$$

For $t_{max} = 10^{-3}$ s, $\sigma_{min} = 0.01$ S/m, $\Delta s_{min} = 15$ m this gives $M \gg 75$. Since in ordinary arithmetics the orthogonality of the vectors q_j breaks down after 20 to 30 iterations (Lanczos phenomenon), the number of required iterations significantly exceeds this bound. In numerical expriments with the parameters mentioned above, it was found that $M = 600$ was appropriate.

3.5 Examples

We finnish this section with two examples.

- The first example (Fig. 4) is the same 1D model shown in Fig. 3 with the results of FDTD. It consists of a 330 m thick 10 Ωm-layer at a depth of 30 m immersed in a uniform halfspace of 100 Ωm, terminated at a depth of 480 m by a perfect conductor. The transmitter stands over the center of the conductor. We have taken 64 uniform cubes (grid width 15 m) in x- and y- direction and 32 cubes in z-direction. The crosses show the results of the spectral method for three time lags along a central profile. These results are compared with the analytical 1D model (full lines). The agreement is excellent (except at early time close to the loop, where the initial field computed as in Sect. 1.3 might be inadequate). $M = 600$ subspace iterations were required to obtain convergence for $t = 10^{-3}$ s.

- The next example shows a typical spectrum of the Ritz values ϑ_m for the model of Fig. 3, but with a coarser spacing $\Delta s = 30$ m. The subspace iteration was carried out until $M = 200$. Fig. 5 displays the spectrum for $1 \leq m \leq M = 200$. Most decay constants are of the order of 10^6 1/s, belong to the decay of small gid size eddies and are without significance for time lags $t > 10^{-5}$ s. In this time range only the smaller decay constants contribute, say $m > 150$. Note that there is an isolated smallest decay constant close to zero, which might belong to a potential field $\mathbf{E} = -\nabla\Phi$, being also an eigensolution of the problem. The arbitrarily chosen Ritz vectors for $m = 50$, 100 and 150 are shown in Fig. 6. Displayed is only the field $\dot{B}_z$ in the surface layer, which already gives a good expression of the nature of these modes. Since these modes are generated in a Krylov-Lanczos process by the square loop in the center the domain, they all show this symmetry.

  The mode $m = 50$, displayed in Fig. 6 (top) shows much of the small-scale detail. Thick lines mark the lines $\dot{B}_z = 0$. The regular pattern does **not** coincide with the grid structure (32×32). The decay mode $m = 100$ (Fig. 6, center) shows already more large scale structure. This becomes even more dominant in the mode $m = 150$ in Fig. 6 (bottom).

Conclusion

The finite difference time domain method and the spectral finite difference method are acceptable methods for modelling 3D-transients, where the latter method was found to be more efficient. In both cases, the computational load increases with $\sqrt{t}$, such that the transient late time response is difficult to access (many time steps in FDTD and many iterations in SLDM).

The Lanczos method used here provides a good estimate of the large eigenvalues and the corresponding eigenvectors (decay modes), which unfortunately decay too fast to be of interest for late time. As an alternative one may apply the Lanczos method not to the eigenvalue problem

$$\underline{\underline{A}}\,\underline{x} = \lambda \underline{x},$$

but to the modified problem

$$\underline{\underline{B}}\,\underline{x} = \mu \underline{x} \quad \text{with} \quad \underline{\underline{B}} = (\underline{\underline{A}} - \tau \underline{\underline{I}}_N)^{-1}, \quad \mu = \frac{1}{\lambda - \tau},$$

which has the same eigenvectors as the original problem, but modified eigenvalues (shift and invert technique). In the modified problem the best estimates are obtained for $|\mu| \to \infty$, which corresponds to $\lambda \to \tau$. An important subcase of this method is the case $\tau = 0$, treated by Druskin *et al.* (1999). If interested in late time transients, the number of iterations might be quite small. However, for this decrease of iterations we pay the extra amount of determining in iteration j the vector $\underline{u}_j$ by

$$\underline{u}_j = \underline{\underline{B}}\,\underline{q}_j \quad \text{or} \quad (\underline{\underline{A}} - \tau \underline{\underline{I}}_N)\underline{u}_j = \underline{q}_j,$$

which is a particular 3D-modelling problem.

Fig. 4: Comparison of numerical spectral finite difference 3D-results with analytical 1D-data. Shown are the central profiles over the loop for three time lags. The agreement is acceptable.

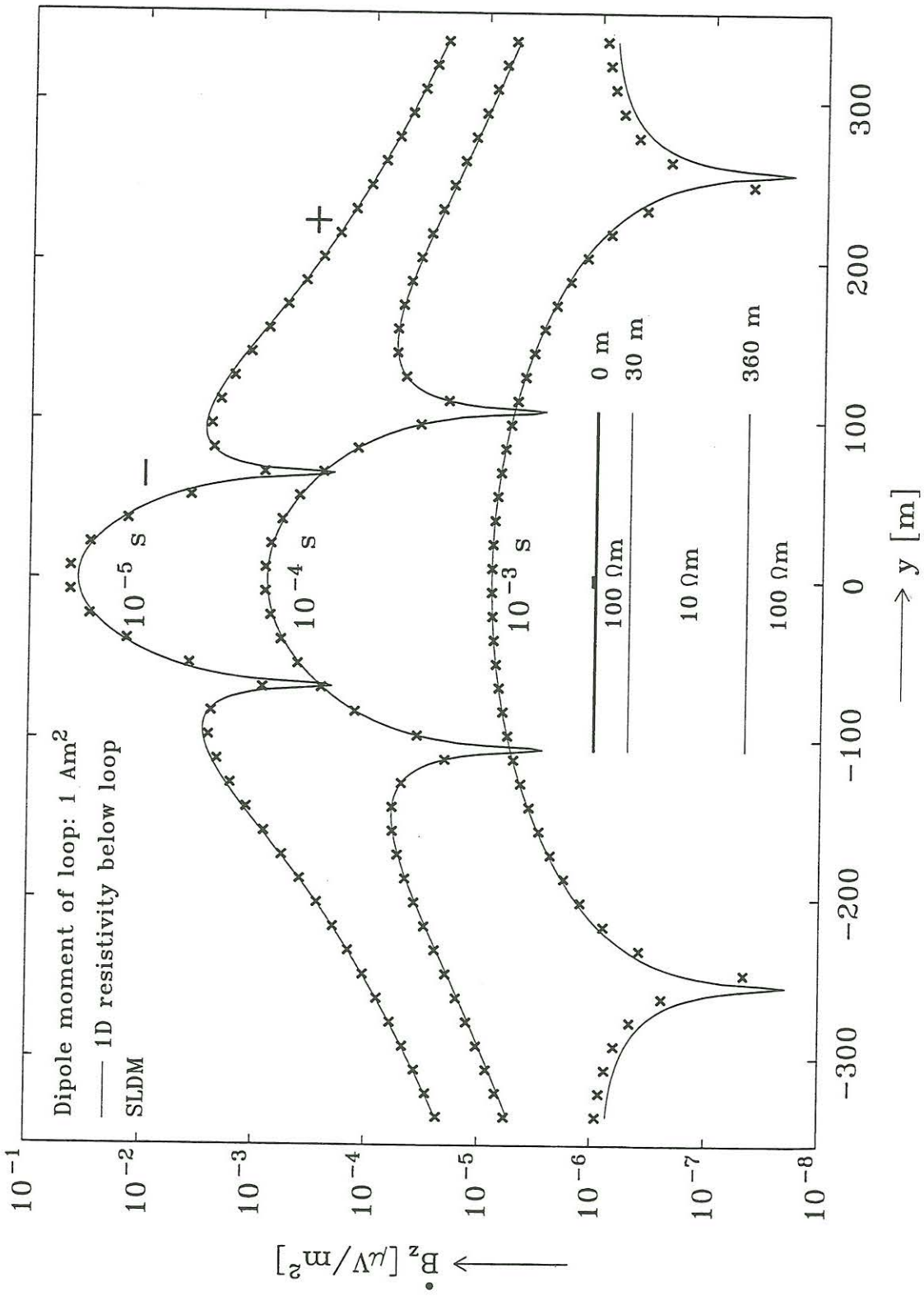

Fig. 5: Typical spectrum of the Ritz values ϑ_m for subspace dimension $M = 200$. Most decay constants describe small grid size eddies. Only the smaller decay constants ($m > 150$) appear be relevant for $t > 10^{-5}$ s.

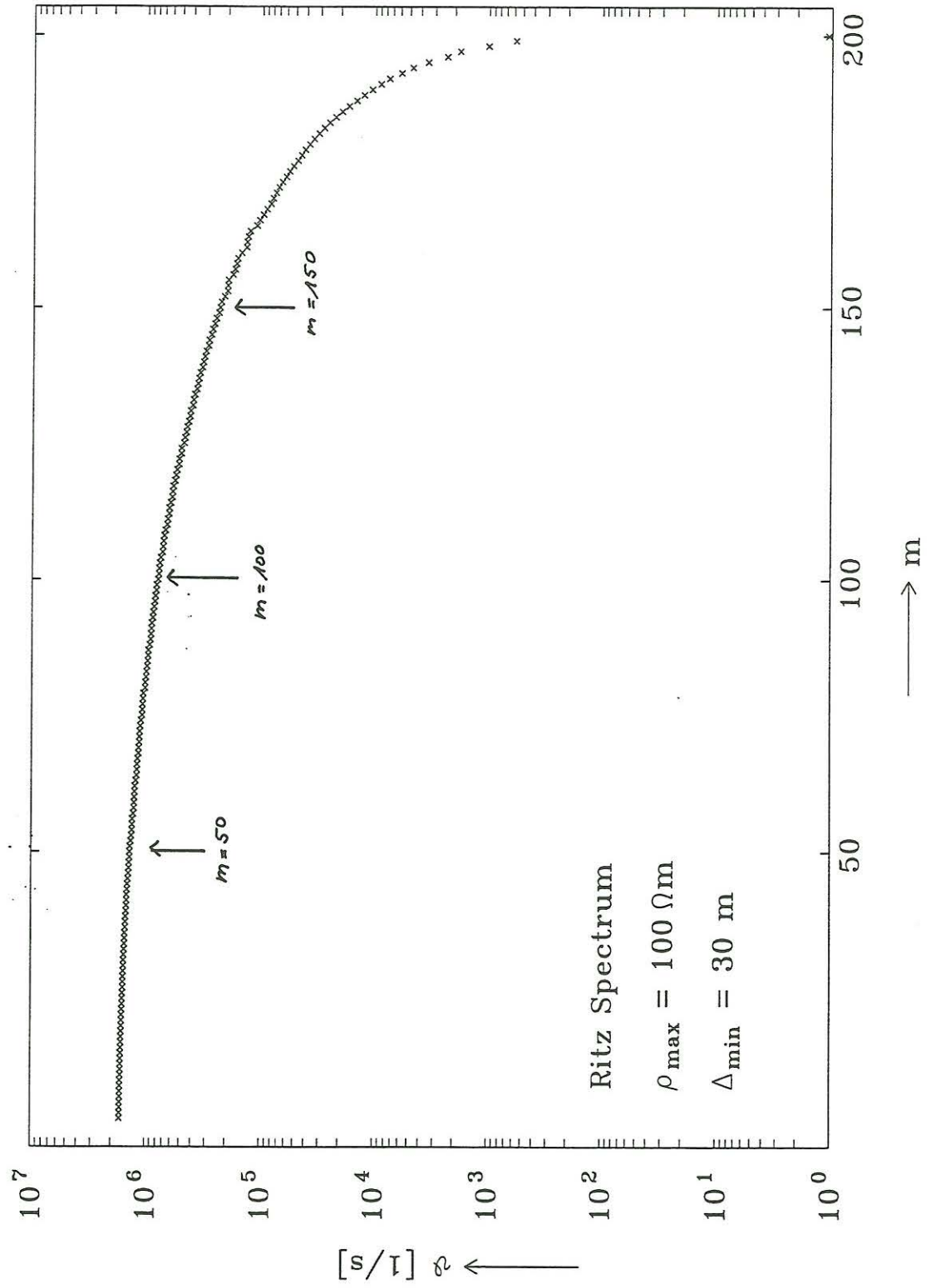

Fig. 6: The Ritz vectors for $m = 50$ (top), $m = 100$ (center) and $m = 150$ (bottom). Displayed is $\dot{B}_z(t)$ at the surface. Thick lines mark the lines $\dot{B}_z = 0$.

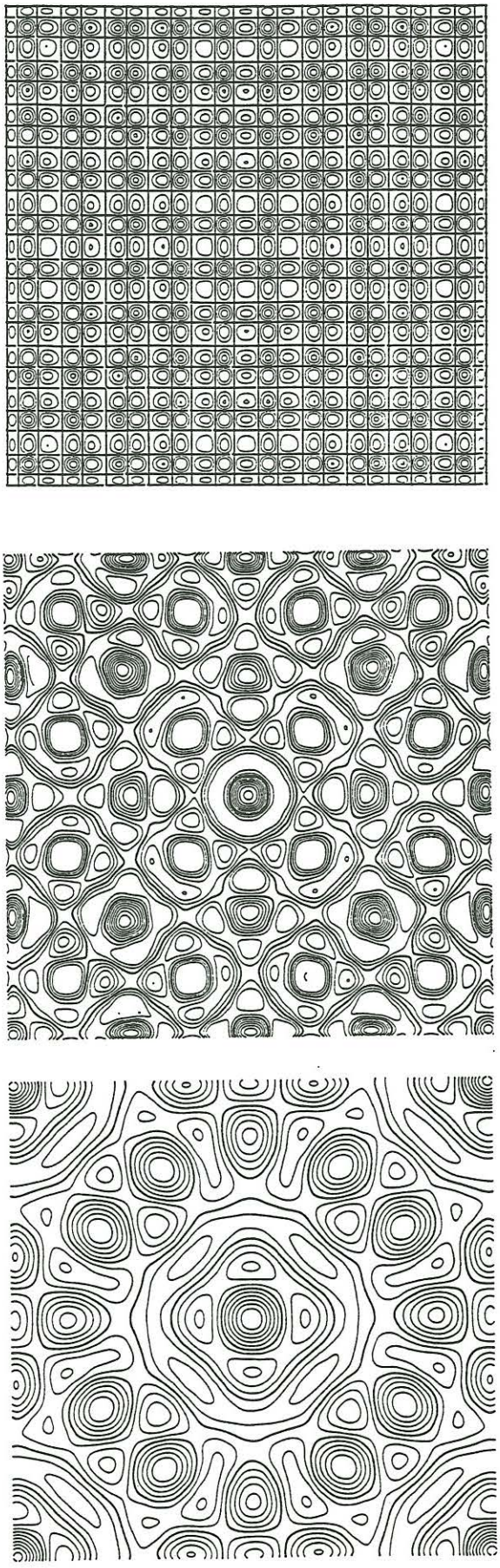

Acknowledgement
I am grateful to Knútur Árnason (Reykjavik) and Boris Singer (Sydney) for encouraging discussions.

References

Adhidjaja, J.I. & Hohmann, G.W., 1989. A finite-difference algorithm for the transient electromagnetic response of a three-dimensional body, *Geophy. J. Int.*, **98**, 233-242.

Árnason, K., 1999. Consistent discretization of electromagnetic fields and transient modeling. *In:* Three-Dimensional Electromagnetics, ed. by M. Oristaglio and B. Spies, *Gephysical Developments*, **7**, Society of Exploration Geophysicists, Tulsa, Oklahoma, U.S.A.

Druskin, V. & Knizhnerman, L., 1988. Spectral differential-difference method for numeric solution of three-dimensional nonstationary problems of electric prospecting, *Izvestiya, Earth Physics*, **24**, 641-648.

Druskin, V. & Knizhnerman, L., 1994. Spectral approach to solving three-dimensional Maxwells's diffusion equations in the time and frequency domains, *Radio Science*, **29**, 937-953.

Druskin, V.L., Knizhnerman, L.A. & Ping Lee, 1999. New spectral Lanczos decomposition method for induction modeling in arbitrary 3-D geometry, *Geophysics*, **64**, 701-706.

Du Fort, E.C. & Frankel, S.P., 1953. Stability conditions in the numerical treatment of parabolic differential equations, *Math. Tables and Other Aids to Computation*, **7**, 135-152.

Grubert, D., 1992. Anwendungen der spektralen finiten Differenzmethode auf Modellrechnungen in der Elektromagnetik, Diplomarbeit, Institut für Geophysik und Meteorologie der Technischen Universität Braunschweig.

Hördt, A., Druskin, V.L., Knizhnerman, L.A. & Strack, K.-M., 1992. Interpretation of 3-D effects in long-offset transient electromagnetics (LOTEM) soundings in the Münsterland area/Germany, *Geophysics*, **57**, 1127-1137.

Moler, C. & van Loan, C., 1978. Nineteen dubious ways to compute the exponential of a matrix, *SIAM Review*, **20**, 801-835.

Oristaglio, M.L. & Hohmann, G.W., 1984. Diffusion of electromagnetic fields into a two-dimensional earth: A finite-difference approach, *Geophysics*, **49**, 870-894.

Parlett, B.N., 1980. The symmetric eigenvalue problem, Prentice-Hall, Inc., Englewood Cliffs.

Remis, R.F. & van den Berg, P.M., 1997. A modified Lanczos algorithm for the computation of transient electromagnetic wave fields, *IEEE Trans. Microwave Theory and Techniques*, **45**, 2139-2149.

Remis, R.F. & van den Berg, P.M., 1998. Efficient computation of transient diffusive electromagnetic fields by a reduced modeling technique, *Radio Science*, **33**, 191-204.

Wang, T. & Hohmann, G.W., 1993. A finite-difference, time-domain solution for three-dimensional electromagnetic modelling, *Geophysics*, **58**, 797-809.

Yee, K.S., 1966. Numerical solution of initial boiundary problems involving Maxwell's equations in isotropic media, *IEEE Trans. Ant. Propag.*, **14**, 302-309.